Resonant photoemission and correlated satellites in K_2CoF_4

Luigi Sangaletti*

Istituto Nazionale per la Fisica della Materia and Dipartimento di Chimica e Fisica per l'Ingeneria e per i Materiali, Università di Brescia, Via Branze, 38-25123 Brescia, Italy

Fulvio Parmigiani

Istituto Nazionale per la Fisica della Materia and Dipartimento di Matematica e Fisica, Università Cattolica, via Trieste 17, 25121 Brescia, Italy

Edward Ratner†

Deutsch Research, 700 E, El Camino Real, Mountain View, California 94040

(Received 21 August 1997; revised manuscript received 12 November 1997)

Resonant photoemission experiments at the Co $3p \rightarrow 3d$ absorption threshold are used to identify the correlated satellites in the one-electron removal spectrum of the valence band of the two-dimensional Ising antiferromagnet K_2CoF_4. In addition, x-ray photoelectron spectra of the core levels, interpreted by a configuration-interaction impurity-cluster model, are reported. The estimated charge transfer Δ and the Mott-Hubbard U charge fluctuations pose K_2CoF_4 in the Mott-Hubbard region of the Zaanen-Sawatzky-Allen diagram. The values of Δ and U are also used to estimate the superexchange parameter J by considering a metal-ligand-metal three-center model. The results for K_2CoF_4 are compared to those obtained for CoO and the effect of Δ on the photoemission spectral features and on the magnitude of J are discussed. [S0163-1829(98)05515-5]

I. INTRODUCTION

The K_2CoF_4 layered perovskite represents one of the archetypes of the two-dimensional (2D) Ising disordered antiferromagnet $K_2Cu_{1-x}Co_xF_4$.[1-11] A proper understanding of the electronic structure, correlation effects and the estimation of the correlation energies in K_2CoF_4 is useful to better describe the underlying coupling mechanisms in the magnetically ordered phases. Indeed, the evaluation of charge transfer and Mott-Hubbard charge fluctuation energies from photoemission data can be used to calculate the superexchange coupling term J in this Ising antiferromagnet and investigate the role of these mechanisms on J.

From the point of view of photoemission spectroscopies, a breakdown of the single-particle description of the electronic structure of K_2CoF_4 is evident from the presence of well-defined resonances of the satellite structures of valence-band photoemission spectra. It turns out that, unless electron correlation effects are properly accounted for, the valence electron behavior of such a narrow-band system cannot be interpreted on the basis of the single-particle eigenvalues derived from one-electron band-structure calculations [Refs. 12–16 and Refs. therein]. Whereas, when many-body approaches, where a configuration-interaction expansion of the many-body states of the interacting systems are properly considered, the correlated satellites should be correctly described.

The present study is aimed to identify and discuss the effect of correlation mechanisms on the electronic structure of K_2CoF_4. In particular, the correlated satellites identified in the valence-band photoemission spectra can be helpful as a reference for theoretical schemes used to calculate quasiparticle spectra starting from energy-band-structure models where strong correlation effects are properly accounted for.

In addition, by contrasting and comparing the electronic properties of these compounds information can be conveyed to the discussion on the effect of the interplay between cation and anion electronic states determining electronic, magnetic and optical properties. In particular, Co-F coordination in K_2CoF_4 is similar to Co-O coordination in CoO. This fact suggests a comparative study of the electronic properties focused onto the role of ligand (O versus F) in shaping the ultraviolet photoelectron and x-ray photoelectron spectra and in determining the strength of the electronic correlations. Within this framework, the effect of covalence and hybridization of the M^{2+}-ligand bond could be evaluated. X-ray photoelectron spectra of the core levels are also interpreted by a configuration-interaction impurity-cluster model. The charge transfer and the Mott-Hubbard charge fluctuations estimated pose K_2CoF_4 in the Mott-Hubbard region of the Zaanen-Sawatzky-Allen (ZSA) diagram.

These results were accomplished by performing x-ray photoemission (XPS) and ultraviolet photoemission spectroscopy (UPS) experiments on K_2CoF_4 single crystals. As for the valence-band data, the use of resonant photoemission (RESPES) and constant initial state (CIS) spectroscopy allowed us to focus on the contribution of Co and F to the one-electron removal valence-band spectrum.

The values of Δ and U are also used to estimate the superexchange parameter J by considering a metal-ligand-metal three-center model composed of a central ligand surrounded by two cations in a 180° geometry. By applying this model also to CoO, the effect of Δ on the magnitude of J is discussed. It is shown that the decrease of J from CoO to K_2CoF_4 is mainly related to the increase of Δ.

II. EXPERIMENT

Transition-metal compounds $A_2M\mathrm{F}_4$ ($A=\mathrm{K,Rb}$; $M=\mathrm{Mn,Fe,Co,Ni,Cu,Zn}$) are ionic crystals with halide-perovskite layered structure. They crystallize in the D_{4h} (Ref. 17) tetragonal space group in the paramagnetic phase. Crystals of these compounds consists of successive $M\mathrm{F}_2$ planes, separated by two $A\mathrm{F}$ planes. Alternatively, the crystal structure can be viewed as a two-dimensional network of transition metal-halogen octahedra, piling up in the crystallographic c axis. $\mathrm{K_2CoF_4}$ has a tetragonal unit cell with lattice parameters $a=4.073$ Å and $c=13.087$ Å.[17] $\mathrm{K_2CoF_4}$ is regarded as a two-dimensional Ising antiferromagnet with a Nèel temperature of 107 K and an exchange energy $J=-97$ meV.[18–20] To the best of our knowledge, very few sources of experimental data are available concerning $A_2M\mathrm{F}_4$ electronic structure (see, e.g., Ref. 21, and references therein). The energy gap of $\mathrm{K_2CoF_4}$ is greater than 5.5 eV, as indicated by optical data.[21]

$\mathrm{K_2CoF_4}$ single crystals were grown by the flux method, under argon/$\mathrm{H_2}$ atmosphere using a mixture of KF and 35 mol % $\mathrm{KCoF_3}$ at a cooling rate of 1 °C h^{-1}. Once grown, the single crystals, several millimetres in size, were controlled by Laue reflection.[21]

XPS experiments were carried out with a Perkin-Elmer Model 5400 spectrometer, equipped with a monochromatic Al-k_α source having a 200×650 $\mu\mathrm{m}^2$ spot size. The pass energy of the analyzer was set to 5.85 eV, which gave an ultimate energy resolution of 0.35 eV, as measured on the $\mathrm{Ag}3d_{5/2}$ core line. Binding energies (BE's) were determined by reference to the Fermi edge of Ag, where the Ag $3d_{3/2}$ core level was set to 368 ± 0.1 eV.

Synchrotron radiation from the SPEAR storage ring, available at the beam line 1-2 of the SSRL Stanford Synchrotron facility was used to perform UPS, CIS, and RESPES measurements in the valence-band energy range. The radiation was dispersed by means of a TGM 6-m monochromator. This system is equipped with three interchangeable gratings, of which the 823 lines/mm, working in the 25–90 eV range, was used. The UPS spectrometer was a VG/ADES 400 equipped with a hemispherical analyzer (angular resolution $\pm2°$). The pass energy of the analyzer was set to give an ultimate energy resolution of 0.5 eV, as measured on the Au Fermi edge. Even better resolution was tried, but that did not enhance our ability to resolve the details of the valence band.

To reduce surface charging an electron flood gun was used during UPS and XPS runs. The energy of the electron beam during the XPS experiments was adjusted in order to minimize the width of the F $1s$ core line. Binding energies of UPS data were measured with reference to the K $3p$ BE, which was set at 18.4 eV.

The samples were cleaved in UHV at a pressure of 2×10^{-10} torr and the pressure inside the chamber during the experiments was better than 3×10^{-10} torr. The fracture surface was identified as the $\langle001\rangle$ surface.

III. RESULTS AND DISCUSSION

Figure 1(a) shows the F $1s$ XP spectrum of $\mathrm{K_2CoF_4}$. The binding energy is 684.4 eV and the full width at half-
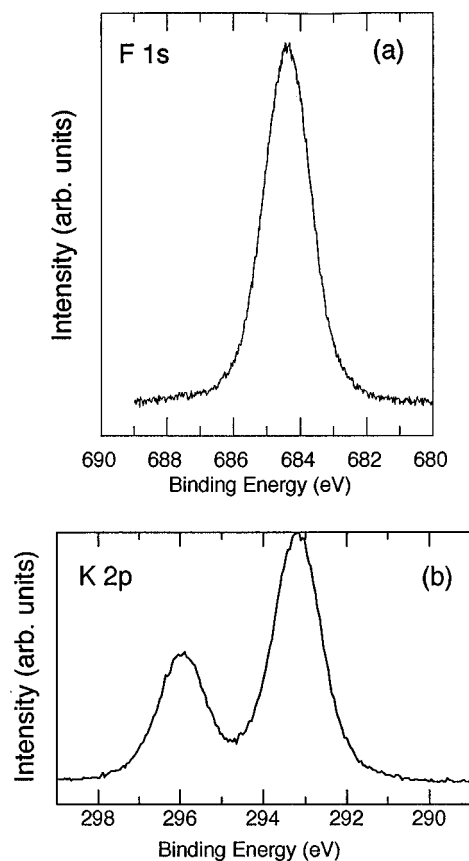
FIG. 1. XPS spectra of the F $1s$ (a) and K $2p$ (b) core levels of $\mathrm{K_2CoF_4}$.

maximum is 1.6 eV. The line shape is symmetric and no satellites on the high-BE side are present. This result suggests a well-ordered K-F cleavage plane.

The K $2p$ XP spectrum is reported in Fig. 1(b). The photoemitted K $2p$ electrons originate a spin-orbit split structure with a low-BE peak at 293 eV and a high-BE peak at 296 eV. No evidence of satellite structures is observed.

In Fig. 2(a) the Co $2p$ XPS spectrum of $\mathrm{K_2CoF_4}$ is shown. Two groups of structures, separated by nearly 17 eV are detected. The group at lower BE is attributed to the Co $2p_{3/2}$ spin-orbit component, while the group at higher BE arises from the Co $2p_{1/2}$ component. Focusing on the Co $2p_{3/2}$ structures, a main line (A) at 780 eV, a satellite (B) at 786.5 eV, and a low-intensity structure (C) at 788 eV can be observed. The spectral structures are similar to the ones observed in highly correlated transition-metal compounds as CoO and Co halides.[22–24] Rather interesting is the comparison with the Co $2p$ core lines of CoO [Fig. 2(b)]. In $\mathrm{K_2CoF_4}$ the core lines appear narrower than in CoO and the main line to satellite intensity ratio (I_A/I_B) is larger than in CoO. The latter feature can be ascribed to a reduced charge transfer energy in CoO with respect to $\mathrm{K_2CoF_4}$. A similar effect was also pointed out in the study of Ni dihalides.[25] Indeed, the main line intensity of the Ni^{2+} XPS spectra was found to increase with the charge-transfer energy. Therefore the more ionic $\mathrm{NiF_2}$ compound has a larger I_A/I_B ratio than the less ionic $\mathrm{NiI_2}$ and $\mathrm{NiBr_2}$ compounds. This trend can be easily discussed on the basis of parametrized configuration-interaction impurity-cluster models.[26]
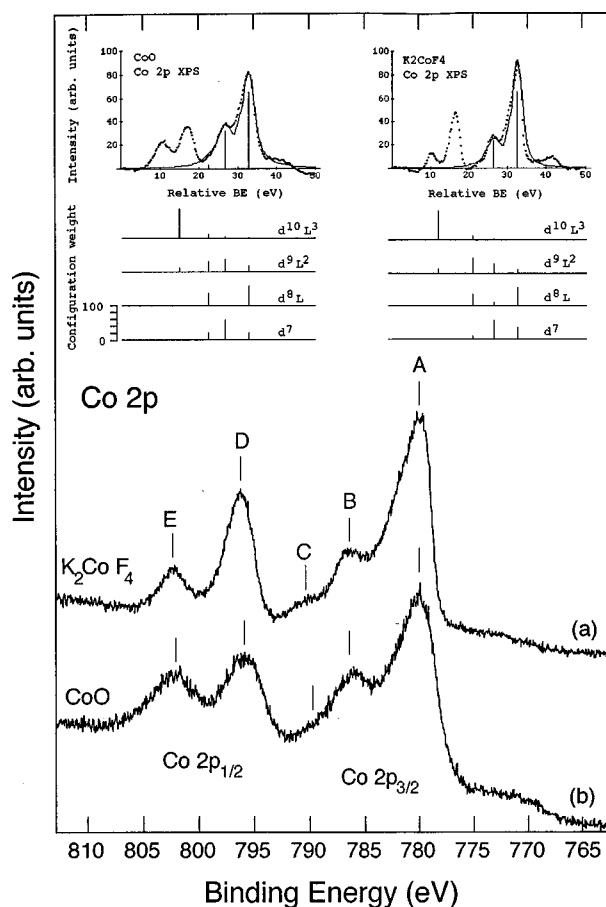
FIG. 2. XPS spectra of the Co $2p$ core levels of K_2CoF_4 (a) and CoO (b). Inset: results of the parametrized CI impurity cluster calculations of the Co $2p_{3/2}$ core levels of K_2CoF_4 (right) and CoO (left).

The Co $3s$ core-level spectrum of K_2CoF_4 is shown in Fig. 3(a). Three features are clearly detectable: a main line (A) at 105 eV, a broad peak (B) at 110 eV, and a feature (C) on the high BE side (116 eV). In Fig. 3(b) the Co $3s$ XPS spectrum of CoO is also shown. As in the case of Co $2p$ core levels, the spectral features are broader than in K_2CoF_4 and the main line to satellite intensity ratio (I_A/I_B) is larger.
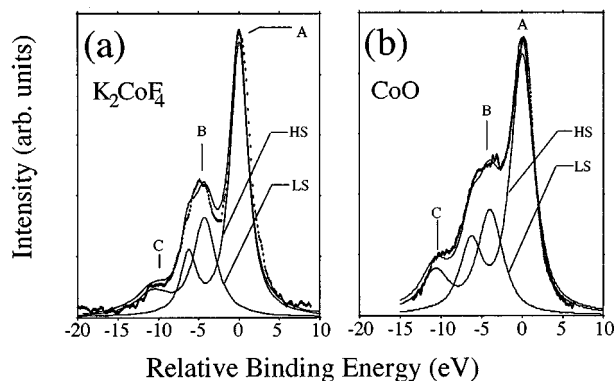
FIG. 3. XPS spectra of the Co $3s$ core levels of K_2CoF_4 (a) and CoO (b). Below each spectrum the $3s$ spectra calculated on the basis of the CI impurity cluster model are reported. HS (LS) refers to the high-spin (low-spin) contribution to the final state.
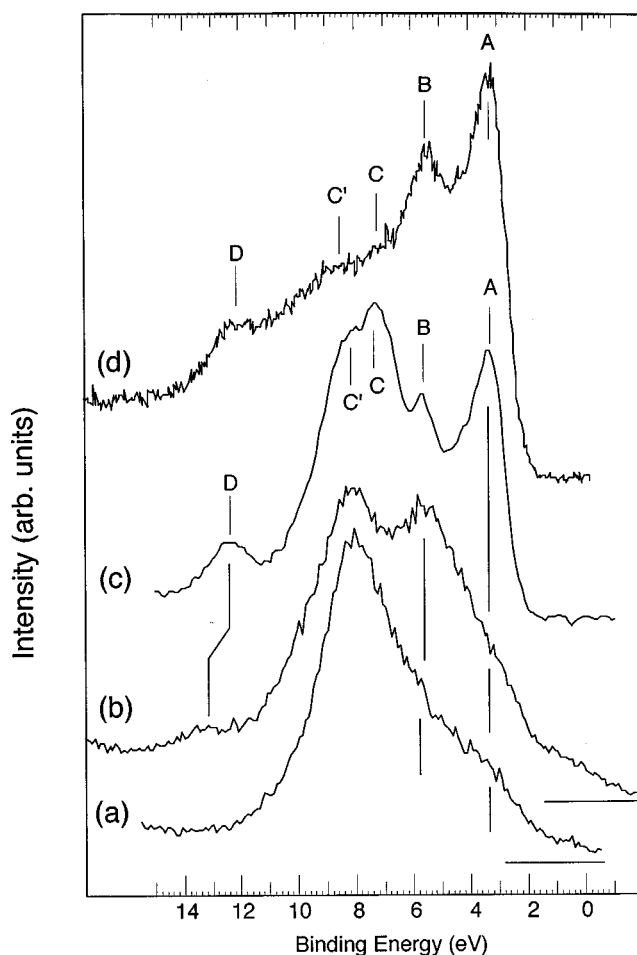
FIG. 4. UPS spectra in the valence-band region of K_2CoF_4 with a photon energy of 58 eV (a) and 63 eV (b). One-electron removal valence-band XPS spectrum of K_2CoF_4 (c) and CoO (d).

Figure 4 shows the UPS [$h\nu=58$ eV (a) and 63 eV (b)], and XPS [Al k_α (c)] one-electron removal valence-band spectra of K_2CoF_4. The CoO XPS spectrum in the valence-band region is also shown [Fig. 4(d)]. The XPS spectrum of K_2CoF_4 shows a peak (A) at 3.5 eV followed by a structure (B) at 5.8 eV and a broad structure (C-C') extending from 6 to 11 eV with the maximum at 7.3 eV. An additional spectral line (D) can be observed at 12.4 eV. Quite similar spectral features are detectable in the CoO XPS spectrum. The main difference between the two compounds is found in the spectral intensity in the 5–11 eV region, which could be ascribed to the larger ligand to Co (L:Co) stoichiometric ratio in the perovskite (4:1) with respect to the oxide (1:1).

The UPS spectra were collected at photon energies of 58 eV, in order to minimize the Co$3d$/F$2p$ photoemission cross section.[27] This procedure would, in principle, allow us to evidence the F $2p$ contribution to the valence band. Actually, the sharp emissions (A and B) observed in the XPS spectrum are quenched, while the broad band in the 5–11 eV BE range still appears, even though a considerable loss of weight is observed in the energy region corresponding to feature C. These findings suggest that there exists some strong dependence of the spectral features on the photon energy. Indeed, the UPS spectrum collected at $h\nu=63$ eV [Fig. 4(b)] presents a strong enhancement of the spectral weight at approxi-

mately BE=6 eV. The UPS data also show a weak emission in the 0–2 eV range, which is not found in the XPS spectrum. Due to the higher surface sensitivity of the UPS probe, this emission is ascribed to surface/defect states. The better quality of the XPS data is due to the much narrower photon beam spot on the sample surface in the case of XPS photoemission (200×350 μm^2) with respect to the synchrotron beam (1×1 mm^2), which allowed us to choose an optimal sample region by minimizing defect-related features in the energy-gap region of the XPS spectra.

In the light of the results shown in Fig. 4, peaks A, B, C, and D in the XPS spectrum are ascribed to the Co contribution, while the spectral weight in the 7–11 eV region (roughly corresponding to peak C') is ascribed to the F contribution. Indeed, at x-ray photon energies the atomic cross section for the $3d$ bands is larger than the atomic cross section for $2p$ bands,[27] whereas the reverse is reported at the UV photon energies. Observations based on this simplistic argument would suggest that at higher photon energies the one-electron removal valence-band spectrum receives the main contribution from $3d$ bands, whereas at UV photon energies the main contribution is given by the $2p$ bands. However, the emission in the valence-band one-electron removal spectrum is far to be described by a pure atomic picture since the $2p$-$3d$ hybridization can introduce states with a strongly mixed character. Therefore, the comparison between the features of valence-band electron removal spectra collected at different photon energies can not be regarded as unambiguous evidence of their character. For this reason RESPES, CIS, and the comparison with other Co^{2+} compound data as well as theoretical results can be helpful to identify the spectral features in the valence band.

It is also worth observing the close similarity between the fine structure (A, B, C, C', and D features) of the two XPS spectra of Fig. 4. This finding suggests that, apart from intensity differences ascribed to the ligand-state contribution in the 7–11 eV range, the energy distribution of the peaks related to Co-$3d$ orbitals is spread all along the valence-band (VB) region and is also rather similar.

As compared to CoO [Fig. 4(d)], the spectral weight between the C-C' and D structures in K$_2$CoF$_4$ [Fig. 4(c)] is lower, which may indicate a minor dispersion of the F $2p$ band with respect to O $2p$ bands.

Finally, a shift towards higher BE's of the satellite D is observed in the UPS spectra [Fig. 4(b)] as compared with the XPS spectrum [Fig. 4(c)]. Shifts in the satellite energy were also observed in NiO and related to energy dispersion effects.[28]

Figure 5 shows the valence band and K $3p$ region as detected by UPS measurements at different photon energies from 58 to 90 eV. The spectra have been normalized according to the calculated K $3p$ photoemission cross section dependence on the photon energy.[27] Resonance effects are clearly observed in the 2–6 eV BE region, as well as in the 12–15 eV BE region, for photon energy ranging from 63 to 72 eV. These energies correspond to the Co $3p \rightarrow$ Co $3d$ absorption threshold. The observed enhancement of spectral weight is due to the resonance between the direct photoemission and the Auger-like channels at this absorption threshold. For the Co^{2+} cation, resonant photoemission involves two channels:
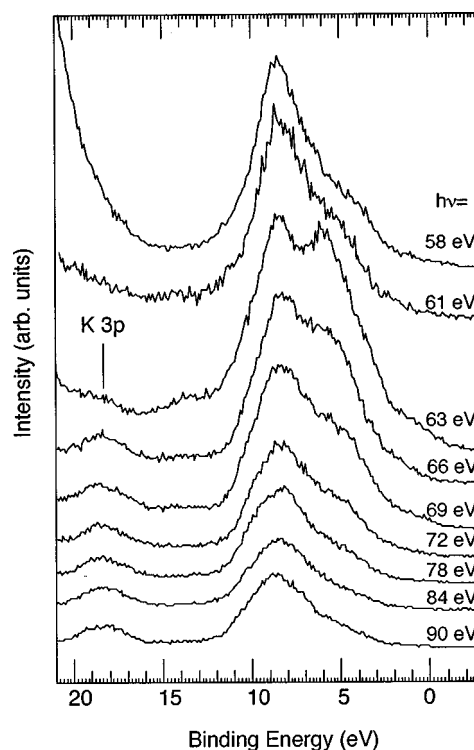
FIG. 5. UPS one-electron removal valence band and K $3p$ spectra of K$_2$CoF$_4$ collected by using synchrotron radiation at different photon energies (from 58 up to 90 eV).

$$ \text{(i)} \quad 3p^6 3d^7 + h\nu \rightarrow 3p^6 3d^6 + e^-, \tag{1} $$

$$ \text{(ii)} \quad 3p^6 3d^7 + h\nu \rightarrow 3p^5 3d^8 \rightarrow 3p^6 3d^6 + e^-. \tag{2} $$
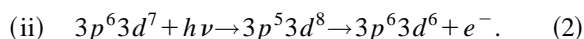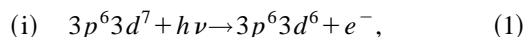
The first channel is the direct photoemission channel, while the second channel, which will open as the photon energy reaches the $3p$ to $3d$ absorption threshold, is an Auger decay following a photoabsorption process. The final states of these channels are indistinguishable so that a quantum interference between them occurs. As a result of the interference, the Co features are enhanced or suppressed at the absorption threshold near 60 eV.

A closer view to the resonance effect is presented in Fig. 6, where CIS and RESPES spectra are shown. CIS spectra were collected at an initial energy of 5 eV (main line, B) and 14 eV (satellite, D), as indicated by the arrows. As can be observed, both structures resonate, though at different extents and at slightly different photon energies. In particular, the main line resonance is much broader than the satellite resonance. This could be ascribed to a larger Co-F hybridization in the states contributing to the main line and, therefore, to a larger dispersion of the band available for the final state in the absorption process. Though these results are qualitatively similar to what already observed in, e.g., K$_2$NiF$_4$,[29] some differences should be mentioned. In particular, the resonance effect at the $3p \rightarrow 3d$ threshold is much more evident as compared to that observed in Cu^{2+} and Ni^{2+} compounds. This effect is ascribed to the larger density of empty d bands in Co^{2+} than in Ni^{2+} and Cu^{2+}.

It is also rather interesting to observe that the main line of the spectrum collected at 63 eV does not correspond to the main line of the XPS spectrum [peak A, Fig. 4(c)]. In fact,
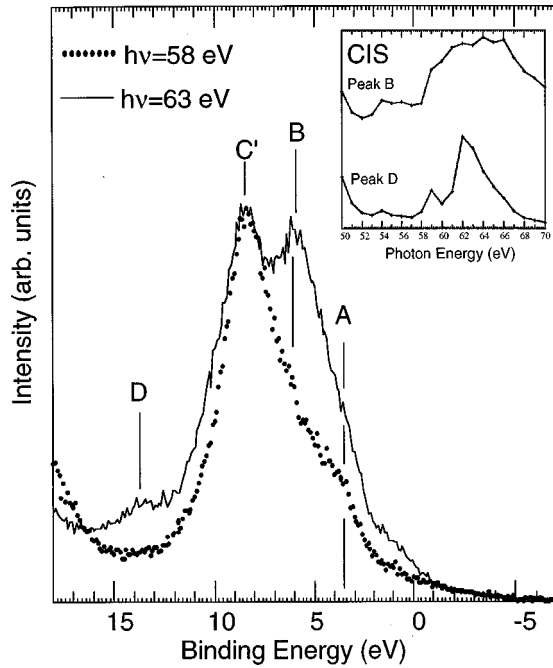
FIG. 6. UPS one-electron removal valence band and K $3p$ spectra of K_2CoF_4 collected on resonance ($h\nu = 63$ eV) and off resonance ($h\nu = 58$ eV) at the Co$3p \rightarrow$ Co$3d$ absorption threshold. Inset: Constant initial state (CIS) spectra measured on the main line (M) and on the satellite (S) of the resonant spectrum.

the strong resonance at $h\nu = 63$ eV corresponds to peak B in the XPS spectrum. Assuming that the more ionic (i.e., $3d^6$) configurations are those yielding a larger resonance, the intensity enhancement of peak B allows us to associate a large $3d^6$ weight to this spectral feature. Also, the resonance of the C band seems to follow the behavior of B, though to a minor extent, and therefore a significant $3d^6$ configuration weight should contribute to this spectral feature. The comparison between UPS and XPS spectra of K_2CoF_4 (Fig. 4) also shows that peaks A and D have similar dependence on photon energy, i.e., both are quenched in the UPS regime and both are clearly detectable in the XPS regime. Therefore, similar configurations weights are assumed to contribute to these bands and, because of their smaller resonance enhancement with respect to peak B, they should present also a significant $3d^7\underline{L}$ configuration weight.

The comparison with the CoO RESPES data[22] allows us to make additional remarks on the character of the spectral features involved in the one-electron removal valence-band spectra. Shen and co-workers[22] have identified a main line at BE$=1$ eV and a satellite at BE$=9.5$ eV, which they ascribed to Co states. A clear enhancement at the resonance was observed for the satellite, to a higher extent with respect to that observed for K_2CoF_4 (feature D, Fig. 4). The main line also shows a remarkable resonance, unlike the main line of K_2CoF_4 [feature A, Figs. 4(a) and 4(b)]. Therefore a different behavior at the $3p \rightarrow 3d$ threshold is shown by the two Co^{2+} compounds. While in K_2CoF_4 the central region (peaks B and C) of the spectrum strongly resonate, in CoO the peaks located outside this region show a more pronounced resonant behavior. This may indicate a different distribution of the configuration weight throughout the valence-band

spectral range. We can assume that the more resonating d^6-like configuration has a higher weight in the central region of the K_2CoF_4 spectrum whereas it is found to contribute more significantly to the low-BE (1 eV) and high-BE (9–10 eV) regions of CoO. The central region of the CoO valence band also presents a nondispersive structure at BE$=3.5$ eV, which can be ascribed to Co states, similar to peak B for K_2CoF_4 (Fig. 4). However, the resonant behavior of this peak in CoO is less evident than in K_2CoF_4.

A comparison between the XPS and RESPES results allows us to draw the following conclusions. (a) The main line A and the peaks B, C, and D observed in the XPS data are ascribed to Co $3d$ states. A significant weight of $3d^7\underline{L}$-like configurations is expected for A and D structures, while the $3d^6$ weight seems to be localized in the midregion of the valence band (B and C). (b) Assuming the energy of peak C' as a reference for the F band centroid and that of peak A for the Co band an increase ($\Delta E \sim 1.3$ eV) of the energy separation between these states is observed with respect to K_2NiF_4.[29] The same increase was found in the case of NiF$_2$ and CoF$_2$.[30]

IV. PARAMETRIZED CONFIGURATION-INTERACTION IMPURITY CLUSTER CALCULATIONS

Calculated photoemission spectra were obtained by applying the configuration interaction approach to a parametrized cluster model in the impurity limit.[31–35] In the case of open shell $3d$ transition-metal compounds, the electronic configuration of the ground state is given by a linear combination of the $3d^n$ (ionic) and $(3d^{n+m}\underline{L}^m$ (covalent) configurations ($\underline{L}$ represents a $2p$ hole on the ligand). The ground state is determined by three parameters: the d-d Coulomb interaction energy U, the charge-transfer (CT) energy Δ, and the hybridization energy T. In the final state a core, or valence, hole is present that strongly couples to the $3d$ states via the coulomb (Q) and the exchange interactions. The spectral weight is calculated according to the formula

$$\rho(e_k) \propto |\langle \psi_c | \hat{r} | \psi_k \rangle|^2 \sum_{i=1}^{n} |\langle \psi_i^f | \underline{c} \psi_{GS} \rangle|^2 \delta(h\nu - e_k - E_i), \quad (3)$$

where $\hat{r}$ is the dipole operator, e_k is the photoelectron kinetic energy, ψ_c is the single-particle wave function in the initial state, ψ_k is the photoemitted (free) electron wave function, ψ_i^f is the final-state wave function of the N-1 electron system, $\underline{c} \psi_{GS}$ is the ground-state wave function of the N-1 "frozen" electron system, $h\nu$ is the photon energy, and E_i is the eigenvalue corresponding to ψ_i^f. The sum is carried out on all the (n) configurations that are necessary to describe the system, including the charge-transfer-derived configurations with the proper symmetry.

For the Co^{2+} cation in the K_2CoF_4 lattice a ^4F ground state is assumed. This configuration is indicated as $|3d^7; ^{2S+1}\Gamma\rangle$, where $^{2S+1}\Gamma$ is the configuration symmetry. Additional configurations can be present in the initial state, which mix with the ionic $|3d^7; ^{2S+1}\Gamma\rangle$ configuration to an extent depending on the degree of ionicity of the Co-ligand

TABLE I. Results of the CI parametrized cluster calculation. The parameter values for CoO and K_2CoF_4 are reported for the Co $3s$ core levels and for the Co $2p$ core levels. All energies in eV. The intensity ratio I_A/I_B between the main line (A) and the satellite (B) in the Co $2p_{3/2}$ spectra (Fig. 2) are also reported, along with the weight of the ionic $\underline{c}3d^7$ configuration in both peaks A and B.

			$3s$ core levels					$2p$ core levels		
	Δ	U	T	Q_{sd}	$EX(d^7)$	$EX(d^8\underline{L})$	Q_{pd}	I_A/I_B	$\underline{c}3d^7$ Peak A (%)	$\underline{c}3d^7$ Peak B (%)
CoO	5.7	5.1	2.0	5.8	5.5	3.6	7.2	1.97	21	58
K_2CoF_4	7.5	4.5	2.0	5.8	5.5	3.6	7.2	2.92	34	57

bonding. These configurations are usually indicated with $|3d^8\underline{L};^{2S+1}\Gamma\rangle$ (single CT screened) and $|3d^9\underline{L}^2;^{2S+1}\Gamma\rangle$ (double CT screened).

When core holes are created, depending on the symmetry of the hole, the final-state configurations result from the coupling of the ground state with the hole left behind by the photoelectron. This coupling gives rise to a set of final-state configurations denoted as $|\underline{c}3d^{7+m}\underline{L}^m;^{2S+1}\Gamma_f\rangle$. In particular, in the case of $3s$ core holes (a_{1g} symmetry), the final-state configurations $^{2S+1}\Gamma_f$ are ^5F [high spin (HS)] and ^3F [low spin (LS)].

The result of the Co $3s$ data fitting is shown in Fig. 3. Two groups of emissions contributed to the $3s$ spectral weight. One comes from the HS states, the other from the LS states. Both groups involve ionic and screened configurations. The separation between the centroids of these groups is related to the exchange energy, $K(3s,3d)$, resulting from the Co $3s$–Co $3d$ electron interaction. This separation is roughly one half of the expected value $K(3s,3d)$.[36] Indeed, by defining the parameter EX as the energy difference between corresponding configurations in the HS and LS final states $(EX(d^7)=\langle d^7|H_{HS}|d^7\rangle - \langle d^7|H_{LS}|d^7\rangle$ and $EX(d^8\underline{L})=\langle d^8\underline{L}|H_{HS}|d^8\underline{L}\rangle - \langle d^8\underline{L}|H_{LS}|d^8\underline{L}\rangle$, where H_{HS} (H_{LS}) represents the Hamiltonian matrix in the HS (LS) final states[35]), the EX values relative to the HS-LS splitting obtained from the data fitting are EX=5.5 eV for the $3d^7$ configurations and EX=3.6 eV for the $3d^8\underline{L}$ configuration (see Table I). This is a well-known effect, which is ascribed to the presence of configurations resulting from the near degeneracy of electronic levels in the Co M shell and is observed in late transition-metal (TM) $3d$ monoxides (Refs. 35 and 37 and references therein). Table I also reports the values of the charge transfer (Δ), hybridization (T), core hole–$3d$ electron Coulomb interaction (Q_{sd}), and $3d$-$3d$ Coulomb interaction (U) parameters. The error-bar for the hybridization energy is ±0.25 eV, while that of the other parameters is ±0.5 eV. On the basis of the parameters obtained from the $3s$ core-level analysis, the fitting of Co $2p$ XPS data was carried out. The $2p$ core hole is not total-symmetric as in the $3s$ case, therefore coupling between the $3d$ electrons and the $2p$ core hole give rise to a larger number of configurations. Therefore we have considered only four configurations in the case of Co $2p$ electron emission and only the value of Q was changed in the data fitting (Q_{pd} in Table I), which resulted to be, as expected, greater than Q_{sd}. The results are shown in the inset of Fig. 2. On the basis of the parameter values of Table I, K_2CoF_4 can be classified as a Mott-Hubbard insulator within the Zaanen-Sawatzky-Allen scheme[38] (Δ

=7.5 eV> U=4.5 eV), whereas CoO is placed in the intermediate region of the ZSA diagram, in agreement with the classification proposed by van Elp *et al.*[39] and based on the results of the analysis of one-electron removal valence-band spectra.

However, the relative magnitude of Δ and U do not tell us much about the nature of the lowest ionization state in these materials. When an electron is removed from the valence band it may have either a d-like character [d^{n-1} photoemission spectroscopy (PES), final state] or a p-like character (d^np^5 PES final state). When an electron is added to the empty states, which in $3d$ TM oxides present a d-like character, a d^{n+1} state is obtained [lowest level in the final state of inverse photoemission spectroscopy (IPES)]. Depending on the nature of the PES final state the following excitations are therefore allowed:

$$d^{n-1}\xrightarrow{U}d^{n+1} \quad \text{(Mott-Hubbard type)},$$

$$d^np^5\xrightarrow{\Delta}d^{n+1} \quad \text{(charge-transfer type)}.$$

In a schematic picture where the hybridization energy T is set to zero the charge-transfer regime occurs when Δ, the energy difference between the d^np^5 state and the d^{n+1} state, is lower than U, the energy difference between the d^{n-1} state and the d^{n+1} state. If $\Delta\approx U$ the compound is classified in the intermediate regime and for $\Delta>U$ in the Mott-Hubbard regime. When $T\neq0$, strongly hybridized states can be pushed below the d^np^5 states in the final state of the photoemission process and the lowest ionization state can acquire a lot of $3d^{n+p}\underline{L}^p$, i.e., charge transfer, character.[40] Thus, states previously ascribed to d^{n-1} configurations (d-like states) can be found, hybridized with ligand orbitals, as the lowest ionization states as is the case of K_2CoF_4 and the d^{n-1} configurations are no more pure d-like states. This may help us to understand why K_2CoF_4, where a significant weight of the $3d^7\underline{L}$-like configurations is expected for the A peak (Fig. 4) in the one-electron removal valence-band photoemission spectra, can be regarded as Mott-Hubbard insulator.

V. MAGNETIC PROPERTIES

The parameters obtained from the XPS data analysis can be used to gain also a qualitative understanding of the magnetic properties. To this purpose, the configuration interac-

TABLE II. Results of the calculation relative to the antiferromagnetic exchange energy J. z is the number of magnetic nearest neighbors, S the total spin in the ground state, T_N the Nèel temperature, and J the superexchange coupling term. The charge fluctuation parameters Δ and U are taken from Table I.

	$T_{N,exp}$ (K)	J_{exp} (K)	z	S	Δ (eV)	U (eV)	T (eV)	$T_{N,calc}$ (K)	J_{calc} (K)
CoO	271		6	3/2	5.7	5.1	$1.6/\sqrt{3}$	280	
K$_2$CoF$_4$	108.75	-95.1[a]	4	3/2	7.5	4.5	$1.6/\sqrt{3}$	108.8	-98

[a]$J_\parallel = J$ coupling in the a-b plane.

tion approach to the Anderson Hamiltonian in the impurity limit was applied to a TM-L-TM cluster (TM=Co, L=O,F) with the aim to estimate the superexchange integral J and the Nèel temperature in CoO and K$_2$CoF$_4$.

Magnetic insulators have been treated in the past with the Anderson superexchange theory.[41] It has been shown, however, that when charge-transfer excitations are properly accounted for, better estimates of the Néel temperatures for transition-metal monoxides are given.[42,43] Zaanen and Sawatzky proposed, on the basis of the configuration interaction scheme, the simplest three-center d_i-L-d_j (where i and j indicate different cation lattice sites) superexchange model including charge transfer excitations.

The problem can be solved numerically, but also approximate solutions are often given and discussed (see, e.g., Ref. 44 and references therein). By considering the approximate solution

$$J \simeq -2(T/\Delta)^2(1/\Delta + 1/U)$$

one can appreciate the difference with respect to the Anderson expression for J when charge-transfer mechanisms are accounted for. In the present case, the factor $1/U$ appearing in the Anderson expression is substituted by $1/U + 1/\Delta$. Since in NiO and CoO $\Delta \approx U$ and in HTSC cuprates and related compounds $\Delta > U$, it becomes evident that in these compounds the charge-transfer energy strongly affects their magnetic properties.

According to Zaanen[43] the Nèel temperature T_N can be expressed as

$$T_N = 2JzS(S+1)/(3k_B n^2)$$

where z is the cation coordination number, S the cation spin in the ground state, k_B the Boltzmann factor, and $n = 2S$.

The results for CoO and K$_2$CoF$_4$, obtained by numerically solving the energy matrixes for the TM-L-TM cluster,[44] are reported in Table II. The value of the hybridization integral was set at $T = 1.6/\sqrt{3}$, as suggested by Zaanen.[44] The excellent agreement we find with the experimental results can, to some extent, be accidental because the values of Δ and U resulting from the analysis of photoemission data have been used for the calculation of J, without considering that these values are referred to the N-1–electron final state of the photoemission process and corrections are needed to estimate the values for the N-electron ground state.[45–47] However, the present results make it possible to comment on the effect of Δ on the value of superexchange for the two Co^{2+} compounds. Since the U energies of CoO and K$_2$CoF$_4$ are similar

(Table I), the J energy is lowered from CoO to K$_2$CoF$_4$ by the increase of Δ, while T_N is further decreased by the decrease of z from 6 to 4.

VI. CONCLUSIONS

The electronic structure of the 2D Ising antiferromagnet K$_2$CoF$_4$ has been studied by photoelectron spectroscopy. The analysis of the Co $2p$ core-level data carried out with a parametrized configuration interaction impurity cluster model has shown that K$_2$CoF$_4$ can be regarded as a Mott-Hubbard insulator. In fact, due to the ionicity of the Co-F bond the F $2p \rightarrow$ Co $3d$ charge-transfer energy is larger than the U energy. This finding can also be qualitatively appreciated by considering the main line to satellite intensity ratio I$_A$/I$_B$ in the core-level data (Table I). The higher ionicity of the Co-F bond with respect to the, e.g., Co-O bond results in an increase of I$_A$/I$_B$ with the bond ionicity to which the charge-transfer energy is related. This behavior is observed for both the Co $2p_{1/2}$ and Co $2p_{3/2}$ core lines. In particular, for the Co $2p_{3/2}$ core lines goes from 1.97 in CoO up to 2.92 in K$_2$CoF$_4$. The Δ increase results in an increased weight of the ionic $3d^7$ configuration in the core-level main lines (from 21 at % of the peak intensity in CoO to 34 at.% in K$_2$CoF$_4$). This effect is supposed to be present also in the one-electron removal spectrum of the valence band. Indeed, RESPES and CIS measurements have shown a remarkable resonance on the Co $3p$-$3d$ absorption threshold in the main line region—as well as in the central region of the one-electron removal valence-band spectrum—larger than that measured for Cu^{2+} (Ref. 48) and Ni^{2+} compounds[29] where only the so-called correlated satellite in the high-BE region (about 10 eV below the main line) was found to resonate at the $3p \rightarrow 3s$ threshold.

Finally, by using the Δ and U values estimated from the analysis of core-level spectroscopies, the superexchange integral J has been calculated on the basis of a model developed for a simple TM-L-TM cluster.[42,43] Is is shown that the decrease of J from CoO to K$_2$CoF$_4$ is related to the increase of Δ, while further decrease of T_N is ascribed to the decrease of the cation coordination number.

[*]Electronic address: sangalet@bsing.ing.unibs.it

[†]Present address: Synopsys Inc., 700E Middlefield Rd., Mountain View, CA 94041.

[1] J. P. Jamet, C. P. Landee, J. Ferré, M. Ayadi, H. Gaubi, and I. Yamada, J. Phys.: Condens. Matter **8**, 5501 (1996).

[2] Y. Fukumoto and A. Oguchi, J. Phys. Soc. Jpn. **65**, 264 (1996).

[3] M. Miyashita and I. Yamada, J. Phys.: Condens. Matter **4**, 10 061 (1992).

[4] T. Goto, K. Nakao, T. Sakakibara, M. Ito, and I. Yamada, Physica B **177**, 373 (1992).

[5] M. Itoh, I. Yamada, M. Ishizuka, K. Amaya, T. Kobayashi, Kei-ichi Koga, and K. Motoya, J. Phys. Soc. Jpn. **59**, 1792 (1990).

[6] H. Kadowaki, H. Yoshizawa, M. Itoh, and I. Yamada, J. Phys. Soc. Jpn. **59**, 713 (1990).

[7] T. Anbe, Y. Yamaguchi, M. Itoh, I. Yamada, H. Fujii, and M. Hidaka, J. Phys.: Condens. Matter **34**, 5921 (1989).

[8] I. Yamada, T. Anbe, Y. Yamaguchi, and M. Itoh, J. Phys. (Paris), Colloq. **49**, 1489 (1988).

[9] M. Itoh, I. Yamada, T. Sakakibara, and T. Goto, J. Phys. Soc. Jpn. **58**, 684 (1989).

[10] W. A. H. M. Vlak, M. J. van Dort, A. F. M. Arts, and H. W. de Wijn, Phys. Rev. B **38**, 11 659 (1988).

[11] M. Hagen and S. A. Higgins, J. Phys.: Condens. Matter **21**, 2701 (1988).

[12] V. I. Anisimov, P. Kuiper, and J. Nordgren, Phys. Rev. B **50**, 8257 (1994).

[13] M. T. Czyzyk and G. A. Sawatzky, Phys. Rev. B **49**, 14 211 (1994).

[14] T. Mizokawa and A. Fujimori, Phys. Rev. B **53**, R4201 (1996).

[15] C. Calandra and F. Manghi, Phys. Rev. B **50**, 2061 (1994).

[16] F. Manghi, C. Calandra, and S. Ossicini, Phys. Rev. Lett. **73**, 3129 (1994).

[17] D. Babel, E. Herdtweck, Z. Anorg. Allg. Chem. **487**, 75 (1982).

[18] J. Als Nielsen and R. J. Birgenau, Am. J. Phys. **45**, 554 (1977).

[19] R. M. White and T. H. Geballe, *Long Range Order in Solids* (Academic, Boston, 1979), Table VI.5.

[20] Additional references on the magnetic properties of the layered K_2CoF_4 perovskite can be found in J. B. Goodenough and J. M. Longo, in *Magnetic and Other Properties of Oxides and Related Compounds*, edited by W. Martienssen, Landolt-Börnstein, New Series, Group III, Vol. 4, Pt. a (Springer, Berlin, 1970), p. 253.

[21] G. Samoggia, F. Parmigiani, and F. Leccabue, Solid State Commun. **55**, 157 (1985).

[22] Z.-X. Shen, J. W. Allen, P. A. P. Lindberg, D. S. Dessau, B. O. Wells, A. Borg, W. Ellis, J. S. Kang, S.-J. Oh, I. Lindau, and W. E. Spicer, Phys. Rev. B **42**, 1817 (1990).

[23] K. Okada, A. Kotani, J. Phys. Soc. Jpn. **61**, 449 (1992).

[24] J. Park, S. Ryu, Moon-sup Han, and S.-J. Oh, Phys. Rev. B **37**, 1086 (1988).

[25] J. Zaanen, C. Westra, and G. A. Sawatzky, Phys. Rev. B **23**, 4369 (1981).

[26] F. Parmigiani and L. Sangaletti, in *Core Level Spectroscopies for Magnetic Phenomena: Theory and Experiment* (Plenum, New York, 1995), pp. 249–264.

[27] J. J. Yeh and I. Lindau, At. Data Nucl. Data Tables **32**, 1 (1985).

[28] Z.-X. Shen, R. S. List, D. S. Dessau, B. O. Wells, O. Jepsen, A. J. Arko, R. Bartlett, C. K. Shih, F. Parmigiani, J. C. Huang, and P. A. P. Lindberg, Phys. Rev. B **44**, 3604 (1991).

[29] L. Sangaletti, F. Parmigiani, E. Ratner, Z.-X. Shen, C. Chemelli, and O. Jepsen, Phys. Rev. B **50**, 17 854 (1994).

[30] S. P. Kowalczyk, Ph.D. thesis, University of California, Berkeley, 1976.

[31] A. Fujimori and F. Minami, Phys. Rev. B **30**, 957 (1984).

[32] J. van Elp, H. Eskes, and G. A. Sawatzky, Phys. Rev. B **45**, 1612 (1992).

[33] A. Fujimori, M. Saeki, N. Kimizuka, M. Taniguchi, and S. Suga, Phys. Rev. B **34**, 7318 (1986).

[34] A. Fujimori, N. Kimizuka, T. Akahane, T. Chiba, S. Kimura, F. Minami, K. Siratori, M. Taniguchi, S. Ogawa, and S. Suga, Phys. Rev. B **42**, 7580 (1990).

[35] F. Parmigiani and L. Sangaletti, Chem. Phys. Lett. **213**, 613 (1993).

[36] D. A. Shirley, in *Photoemission in Solids I: General Principles*, edited by M. Cardona and L. Ley (Springer, Berlin, 1978), pp. 165–195.

[37] L. Sangaletti, L. E. Depero, P. S. Bagus, and F. Parmigiani, Chem. Phys. Lett. **245**, 463 (1995).

[38] J. Zaanen, G. Sawatzky, and J. W. Allen, Phys. Rev. Lett. **55**, 418 (1985).

[39] J. van Elp, J. L. Wieland, H. Eskes, P. Kuiper, G. A. Sawatzky, F. M. F. de Groot, and T. S. Turner, Phys. Rev. B **44**, 6090 (1991).

[40] J. W. Allen, R. Claessen, R. O. Anderson, W. P. Ellis, C. Janowitz, C. G. Olson, J.-H. Park, L. H. Tjeng, C. T. Chen, P. Metcalf, H. R. Harrison, M. C. de Andrade, E. A. Early, S. Harm, R. F. Jardmin, M. Kalning, L.-Z. Liu, R. Manzke, M. P. Maple, S.-J. Oh, and M. Skibowski, in *The Physics and Mathematical Physics of the Hubbard Model*, edited by D. K. Campbell, J, M. P. Carmelo, and F. Guinea (Plenum, New York, 1994).

[41] P. W. Anderson Phys. Rev. **115**, 2 (1959).

[42] G. A. Sawatzky, in *Earlier and Recent Aspects of Superconductivity*, edited by J. G. Bednorz and K. A. Müller (Springer-Verlag, Berlin, 1990), pp. 345–376.

[43] J. Zaanen, Ph.D. thesis, University of Groningen (1986).

[44] H. Eskes and J. H. Jefferson, Phys. Rev. B **48**, 9788 (1993).

[45] G. Lee and S.-J. Oh, Phys. Rev. B **43**, 14 674 (1991).

[46] J. Zaanen, C. Westra, and G. A. Sawatzky, Phys. Rev. B **33**, 8060 (1986).

[47] J. Zaanen and G. A. Sawatzky, J. Solid State Chem. **88**, 8 (1990).

[48] Z.-X. Shen and D. S. Dessau, Phys. Rep. **253**, 1–162 (1995).